Potential of Clumped Isotopes in Constraining the Global Atmospheric Methane Budget

Potential of clumped isotopes in constraining the global atmospheric methane budget

Edward Chung[a,b], Tim Arnold[a,b]

[a] National Physical Laboratory, Teddington, UK

[b] School of GeoSciences, University of Edinburgh, Edinburgh, UK

Corresponding authors: edward.chung@npl.co.uk, tim.arnold@ed.ac.uk

Atmospheric methane (CH_4) and its isotopic composition trends over the last decades are explained by various flux scenarios, from tropical wetland emission increases through to reductions in global hydroxyl (OH). In this work we develop a modelling framework to assess the potential usefulness of clumped isotope measurements to distinguish between the main drivers of change in the CH_4 burden. We model interhemispheric differences of 0.12 ‰ and 0.38 ‰ and seasonal cycles of 0.02-0.04 ‰ and 0.21-0.32 ‰ for $\Delta^{13}CH_3D$ and $\Delta^{12}CH_2D_2$, respectfully, which is insignificant relative to the uncertainty of measurements that could eventually be made. We show, however, that measurements of $\Delta^{12}CH_2D_2$ specifically could provide constraints for understanding trends in the global total source and sink magnitudes, which has not been possible with the current sets of observables. Changes in OH concentration of 10 % developed across three decades results in a difference of up to 2 ‰ in $\Delta^{12}CH_2D_2$, which would be observable given current measurement uncertainty limits. For this type of global scale analysis we show that measurements of $\Delta^{13}CH_3D$ would be unlikely to provide additional useful information. We suggest an emphasis should now be on developing the methods to make measurements from ambient air samples, followed by measurements of $\Delta^{13}CH_3D$ and $\Delta^{12}CH_2D_2$ from sampling at clean Northern and Southern Hemisphere sites, combined with more accurate and precise laboratory measurements of the clumped kinetic isotope effects relevant for the atmospheric sinks.

This article has been accepted for publication and undergone full peer review but has not been through the copyediting, typesetting, pagination and proofreading process, which may lead to differences between this version and the Version of Record. Please cite this article as doi: 10.1029/2020GB006883.

1 Introduction

Methane (CH_4) is the second most important anthropogenic greenhouse gas (GHG), contributing a radiative forcing between 1750 and 2011 one third of that due to carbon dioxide (CO_2) (Etminan et al., 2016). Its high radiative efficiency but atmospheric lifetime of around a decade (which is short for a strong GHG) means it has potential to make a large impact on shorter time scales (Shindell et al., 2012). Global atmospheric composition monitoring provides a source of information for understanding the balance between sources and sinks of pollutants and reducing the uncertainties in globally integrated flux estimates. Our understanding of CH_4 fluxes, however, are still inadequate owing to the diversity and complexity of sources (both anthropogenic and natural sources) and the spatial heterogeneity and transience of reactants that are responsible for removing CH_4 from the atmosphere.

Proposed emission based drivers of recent atmospheric growth include increase in releases from tropical wetlands (Nisbet et al., 2016), agriculture (Schaefer et al., 2016), the two combined (Schwietzke et al., 2016), and fossil fuel extraction and utilisation (Howarth, 2019; Rice et al., 2016). There is also uncertainty regarding how changes in hydroxyl radical (OH, CH_4's main reactant) might be affecting the CH_4 budget. The hydroxyl radical has a short lifetime (~1 s) and large atmospheric variability, making it difficult to directly monitor global changes that could be responsible the intra-decade changes in CH_4 (Rigby et al., 2017; Turner et al., 2017). Despite the thousands of measurements currently made every year across the globe an unequivocal interpretation of the recent global CH_4 trends remains elusive. Making progress in further constraining the CH_4 budget will require both maintaining and extending strategically placed, long-term, sustainably funded measurements and delivering new techniques that will ultimately add greater value than spatial and temporal extensions of the currently applied methods (Ganesan et al., 2019; Turner et al., 2019).

Different formation, transport, and removal processes can impart distinctive isotopic fractionation on molecules, providing a vital extra layer of information for studying biogeochemical cycling. CH_4 is made up of ten stable isotopologues, however, so far only the bulk isotopic ratios ($\delta^{13}C$ and δD) have been reported in atmospheric samples for understanding the global CH_4 cycle (Howarth, 2019; Nisbet et al., 2019; Nisbet et al., 2016; Rice et al., 2016; Rigby et al., 2017; Schaefer et al., 2016; Schwietzke et al., 2016; Turner et al., 2019; Turner et

al., 2017). Use of δD has been far less prominent than $\delta^{13}C$ owing to fewer laboratories making these measurements and termination of the long term global time series in 2009-2010. These ratios are typically measured by isotope ratio mass spectrometry (IRMS) by initial conversion of CH_4 to CO_2 or H_2 and therefore this type of analysis does not provide information about how isotopes are partitioned amongst the ten isotopologues (in order of likely highest to lowest natural abundance: $^{12}CH_4$, $^{13}CH_4$, $^{12}CH_3D$, $^{13}CH_3D$, $^{12}CH_2D_2$, $^{13}CH_2D_2$, $^{12}CHD_3$, $^{13}CHD_3$, $^{12}CD_4$, $^{13}CD_4$), and in particular, the measurement of isotopologues that are 'multiply substituted' in the rare isotopes (in CH_4's case ^{13}C and D) i.e. for two or more of the rarer isotopes to 'clump' (Eiler, 2007). Owing to their very low abundance it has not yet been possible to measure even the most abundant clumped isotopologues in ambient air samples. The sensitivity of current high resolution IRMS (HR-IRMS) methods would require extraction of CH_4 from up to 500 L air (assuming ~1.9 ppm CH_4 mole fraction samples). Over the last decade, however, numerous studies have demonstrated the diversity in clumped isotopic signatures of sources and the potential for sink reactions in the atmosphere to impart a significant clumped isotopic signal (Douglas et al., 2017; Whitehill et al., 2017). These geochemical, laboratory and experimental studies have led to speculation that clumped isotope measurements of CH_4 in the atmosphere could be useful for constraining the contemporary changes in the atmospheric burden and therefore raising the incentive for this measurement effort (Ganesan et al., 2019; Haghnegahdar et al., 2017; Turner et al., 2019; Whitehill et al., 2017). It is worth noting that the use of laser spectroscopy in measuring isotopologue ratios (for both clumped CH_4 and as a measure of the bulk isotope ratios) is now possible, however, the attainable levels of precision for analysis of natural samples are only now beginning to reach the levels of mass spectrometry techniques (Eyer et al., 2016; Gonzalez et al., 2019; Ono et al., 2014; Rennick et al., 2021; Röckmann et al., 2016).

Of distinct importance for simplifying the interpretation of isotope ratios of CH_4 in the atmosphere is that CH_4 isotopologues do not exchange carbon or hydrogen isotopes and thus the atmospheric signatures can be explained by the unidirectional source and sink fluxes. This contrasts with the interpretation of CO_2 isotopologue ratios that require consideration of strong and rapid exchange of oxygen isotopes with water, most notably the catalysed exchange inside leaves (Welp et al., 2011). Source studies have shown that the clumped isotopes of CH_4 often reflect formation temperatures, with exceptions from freshwater environments, cow rumens, laboratory culture experiments, or mixtures of gases with different origins (Douglas et al., 2017; D T Wang et al., 2015; Young et al., 2016). Studies

of CH_4 destruction have found that the kinetic isotope effect (KIE) for $^{13}CH_3D$ is near-multiplicative based on reactions rates of $^{12}CH_3D$ and ^{13}CH, i.e. changes in $\Delta^{13}CH_3D$ in the atmosphere are driven by emissions magnitudes and associated source signatures. In contrast, theoretical reaction kinetics calculations suggest that the reaction of $^{12}CH_2D_2$ with atmospheric OH and chlorine (Cl) are significantly slower than predicted based on $^{12}CH_3D/^{12}CH_4$ KIEs alone (Whitehill et al., 2017), likely creating a significant positive clumped anomaly in the atmosphere that could be sensitive to changes in the balance of sources and sinks.

In this work, we use a global chemical transport model, with input fluxes tuned using current observations and an inverse method, to calculate the potential for clumped isotopes to interpret observed variations in the recent global CH_4 burden. To date calculations have not considered the constraints already imposed by the CH_4 mixing ratios and bulk isotope ratios on the magnitudes of changes that could be expected in clumped isotopes. To do this we have used an inverse method that enables us to fix the bulk isotope and mixing ratio trends across more than three decades, thus allowing us to model what actual changes in clumped isotopes could be expected. By applying realistic scenarios of changes in sources and sinks we provide a picture of the true added value that clumped isotope measurements could bring for the coming decades, were a monitoring effort made feasible.

2 Definitions and notation

Following previous descriptions of the definitions and terminology for quantifying deviations in clumped isotopologues (Stolper et al., 2014; Z Wang et al., 2004), we define $\Delta^{13}CH_3D$ and $\Delta^{12}CH_2D_2$ using the following equations:

$$\Delta^{13}\mathrm{CH_3D} = \frac{R_{^{13}\mathrm{CH_3D,measured}}}{R_{^{13}\mathrm{CH_3D,stochastic}}} - 1 \qquad \text{(Eqn 1)}$$

$$\Delta^{12}\mathrm{CH_2D_2} = \frac{R_{^{12}\mathrm{CH_2D_2,measured}}}{R_{^{12}\mathrm{CH_2D_2,stochastic}}} - 1 \qquad \text{(Eqn 2)}$$

where, the denominators can be adequately approximated from the measurements of $R_{^{13}\mathrm{CH_4}}$ (= $[^{13}CH_4]/[^{12}CH_4]$) and $R_{^{12}\mathrm{CH_3D}}$ (= $[^{12}CH_3D]/[^{12}CH_4]$):

$$R_{^{13}CH_3D,\text{stochastic}} = R_{^{13}CH_4,\text{measured}} \cdot R_{^{12}CH_3D,\text{measured}} \quad \text{(Eqn 3)}$$

$$R_{^{12}CH_2D_2,\text{stochastic}} = R_{^{12}CH_3D,\text{measured}} \cdot R_{^{12}CH_3D,\text{measured}} \cdot \frac{3}{8} \quad \text{(Eqn 4)}$$

This approach neglects to consider non-stochastic partitioning of the singly substituted isotopologues. However, as explained arithmetically by Stolper et al. (2014), and routinely reported, there is no significant loss in accuracy in using this method within the likely natural range of isotopologue distributions.

$\Delta^{13}CH_3D$ and $\Delta^{12}CH_2D_2$ are traced to the international scales, VPDB (Vienna Pee Dee Belemnite) and VSMOW (Vienna Standard Mean Ocean Water), defined with absolute ratios $R_{^{13}CH_4,VPDB} = 1.12 \times 10^{-2}$ and $R_{^{12}CH_3D,VSMOW} = 6.23 \times 10^{-4}$, respectfully:

$$R_{^{13}CH_4} = \left(\delta^{13}C \quad + 1\right) \cdot R_{^{13}CH_4,VPDB} \quad \text{(Eqn 5)}$$

$$R_{^{12}CH_3D} = (\delta D + 1) \cdot R_{^{12}CH_3D,VSMOW} \quad \text{(Eqn 6)}$$

where, $\delta^{13}C$ and δD are the reported values from atmospheric monitoring and emission source measurements.

3 Inverse modelling of CH_4 isotopologue ratios

3.1 Global inverse model

3.1.1 Atmospheric chemistry transport model (CTM)

We use a box modelling approach based on the AGAGE-12-Box model developed originally in the 1990s and subsequently revised and updated (Cunnold et al., 1994; Rigby et al., 2013). Our version of the box model is composed of four equally sized zonal regions (extratropics and tropics in the NH and SH), and three vertical layers: lower and upper troposphere and stratosphere. Model inputs include emissions and OH fields that can be altered monthly. The model takes in monthly emission and sink capacities of a chemical species as well as its starting mixing ratios, outputting monthly mixing ratios of those species. Further details of the model and the Python code can be found here: https://gitlab.com/luftwache/chung_box_model.

3.1.2 Inverse method

Ensemble Affine Invariant Markov Chain Monte Carlo (MCMC) algorithm is used as the optimisation framework for the inversion (Goodman and Weare, 2010). The main advantage of MCMC is that it can be applied to problems that cannot be easily solved analytically. It is also suitable for solving non-linear problems without the assumption of Gaussian errors. Thus, the solution can be obtained with any probability density functions applied to priors and posteriors. The Affine Invariant method allows one to run an ensemble of MCMC processes in parallel in order to reduce the time required for optimisation. For each new step of the chain, proposed states of the ensemble members are determined by the accepted/original states in the previous step. We use 1000 members in the ensemble with chain length of 2000, of which the last 100 are analysed.

3.2 Inverse model inputs (state variables)

3.2.1 Emissions magnitudes and isotopic source signatures

For the emission field, we combine EDGAR v4.3.2 (Janssens-Maenhout et al., 2017), WetCHARTs (Bloom et al., 2017), Global Fire Emissions Dataset (GFED) v4.1 (van der Werf et al., 2017) and oceanic, termites and geological seepage from Saunois et al., (2016). The first three datasets are gridded while the latter is a global total. For gridded data, we aggregate grid cells to relevant surface boxes for our input into our model as annual means. As these datasets do not cover the full model time period, we duplicate the nearest available data point for the missing time periods apart from GFED v4.1 for the global fire emissions. For GFED v4.1 we duplicate the mean emission between 1998 and 2011 instead as 1997 is marked with unusually high emission due to Indonesian forest fires. The flat global values are annually-repeated and are distributed evenly across the relevant landmass distribution obtained from ISLSCP II Land and Water Masks with Ancillary Data where applicable (JPL, 2013).

For the purpose of consistency and comparison between separate studies our source $\delta^{13}C$, δD and $\Delta^{12}CH_2D_2$ signatures are taken from Haghnegahdar et al. (2017). Note that we use a different source $\Delta^{13}CH_3D$ to Haghnegahdar et al. (2017) for most sources which is explained below. While better estimates could now be sought (e.g. see thorough work by Sherwood et al. (2017)), our aim in this work is to demonstrate the potential use of clumped isotopes and not to generate new conclusions about the current CH_4 cycle. Total source $\delta^{13}C$ and δD are set at

−54.2 ‰ and −295.0 ‰, respectively, and are optimised in the initial inversion. Uncertainties in these $\delta^{13}C$ and δD sources signatures are 10 % of the given values. A fixed value of global source signature of 20.47 ‰ for $\Delta^{12}CH_2D_2$ is used, calculated from the $\delta^{12}CH_2D_2$ given in Haghnegahdar et al. (2017). For sensitivity tests that look at the effect of a pure fossil fuel emission source (Forward_Qff), we use −41.9 ‰, −177.3 ‰ and 8.37 ‰ as the fossil fuel $\delta^{13}C$, δD and $\Delta^{12}CH_2D_2$ signatures, respectively.

Source $\Delta^{13}CH_3D$ is set to reflect more recent empirical measurements that have been made (Douglas et al., 2020; Douglas et al., 2017; D T Wang et al., 2015). We first categorised source sectors from Haghnegahdar et al. (2017) into fossil fuels, natural microbial, anthropogenic microbial and biomass burning. We then prescribed 2.8 ‰ for fossil fuels (Douglas et al., 2017); 2.8 ‰ for natural microbial sources based on the new measurements of freshwater environments (Douglas et al., 2020); 1.0 ‰ for anthropogenic microbial sources based on cow rumen measurements from D T Wang et al. (2015); and theoretical values from Haghnegahdar et al. (2017) for biomass burning. Combining these signatures gave an overall signature of 2.89 ‰. This can be compared to the earlier $\Delta^{13}CH_3D$ source signatures estimates of Haghnegahdar et al. (2017) of 4.22 ‰.

3.2.2 Tropospheric sink

The prior tropospheric OH concentrations are from Spivakovsky et al. (2000), which have a seasonal cycle and are interannually invariant. For our box model we calculate values for the main boxes. The default is considered as the "mean" condition, and the inverse model solved for global annual anomalies from this mean with an associated uncertainty of 20 %. The anomaly variable is set as global to reflect minimal disparity between OH concentrations in the northern and southern hemispheres (Patra et al., 2014). The KIEs calculated by Whitehill et al. (2017) were used and set as constants.

3.2.3 Other Sinks

In tropospheric boxes, CH_4's lifetime is adjusted so that Cl removes ~25 Tg CH_4 $year^{-1}$. The surface boxes are given a soil sink which removes ~28 Tg CH_4 $year^{-1}$, based on information from Saunois et al. (2016). For the stratospheric losses, including those incurred from OH, the global CH_4 lifetime of CH_4 is set as 159.6 years based on Chipperfield and Liang (2013). In the prior, all non-OH sinks are assumed equally distributed across the four semi-hemispheres, apart from soil uptake, which is proportional to the total landmass distribution obtained from

ISLSCP II Land and Water Masks with Ancillary Data (JPL, 2013). The non-OH lifetimes are given 20 % uncertainty for the initial inversion and set constant thereafter. We use a KIE for reaction with Cl reported by Whitehill et al (2017). The KIE for the singly-substituted isotopologues lost to the soil and to the stratospheric processes is from Snover et al. (2000) and Röckmann et al. (2011), respectfully. We do not assume any clumped isotope effect due to stratospheric or soil loss as they have not been studied. Any clumped isotope effect eventually measured will likely have a small impact on the atmospheric isotope composition owing to their relatively small role in the atmospheric CH_4 budget.

3.2.4 Methane mixing ratios and bulk isotope ratios (observables)

Ground-based in situ CH_4 measurements have been made continuously throughout the globe by two major networks: the Advanced Global Atmospheric Gases Experiment (AGAGE) since 1993 and NOAA since 1983 (Dlugokencky et al., 2020; Prinn et al., 2018). These measurements have agreed very well over the entire timeseries of measurement. Owing to the nature of our model setup (Section 3.1) we simplify our analysis to only incorporate the AGAGE measurements that are made in each of the four semihemispheres and average the data from more than one site where necessary. The gap between the model start date (1980) and AGAGE record (1993~1996) is filled with the Coupled Model Intercomparison Project Phase 6 (CMIP6) input data (Meinshausen et al., 2017). To unify the calibration scales, the CMIP6 data are scaled from NOAA GMD scale to Tohoku University scale used by AGAGE network, by dividing them by 1.0003 as done by Meinshausen et al. (2017). The observed ambient bulk isotopic signatures are from the NOAA/INSTAAR network (White et al., 2016; 2017). Since 2010, measurements of δD have been halted, and there we have tried to use another dataset to gain as realistic representation of the δD in the atmosphere as possible. In the northern extra-tropics, we use data from Fujita et al. (2018) and Morimoto et al. (2017) whose measurements are from northern Canada and Svalbard. We also needed a measurement-model uncertainty (for the inversion Section 3.1.2) that reflects an estimate of the analytical uncertainty on the measurement and how well that measurement can reflect a modelled value. To this end, we estimated the measurement-model uncertainty at 1 % of the observed values for the AGAGE measurements, and 2 % for the CMIP6 data, and 0.2‰ and 4‰ for $\delta^{13}C$ and δD datasets, respectfully.

3.2.5 Initial conditions

For mixing ratios in the lower tropospheric boxes, the initial conditions are taken directly from the starting values in the observation vector (see Section 3.2.4). All boxes in the upper troposphere and the stratosphere are prescribed with the same value as the mean of the lower tropospheric boxes. All values are assigned a uniform uncertainty distribution centred around the mean, with the difference between the maximum and minimum bounds being 20 % of the mean. For isotopically singly substituted CH_4, the first available observation is provided as the starting point for the surface boxes. Like the mixing ratios, the boxes in the upper atmosphere start with the surface average. Singly substituted isotopic ratios have a uniform distribution spanning 10 % of the surface average. For the purposes of our simulation between 1980 and 2015 the initial ambient clumped signatures (of which there are currently no observations) were based on steady state estimates taken from running the model multiple times using the posterior state variables from Inverse_base as input (as described in sections 3.2.1 to 3.2.3 above). Based on these runs, we used initial conditions for $\Delta^{13}CH_3D$ and $\Delta^{12}CH_2D_2$ of 3.2 ‰ and 90.0 ‰, respectively.

4 Results and Discussion

4.1 Initial inversion model run

We summarise the suite of inversion and forward model run experiments in the Table 1. We ran an initial inversion, 'Inversion_base', by assimilating the observations into the inversion model. Inversion_base created a posterior set of values for global emissions and deviation from an assumed OH concentration in 1980 (from here termed OH anomaly) between 1980 and 2015 as shown in Figure 1, and source isotopic signatures (provided in the supporting information). The modelled time series of the monthly CH_4 mole fraction, $\delta^{13}C$, δD, $\Delta^{13}CH_3D$ and $\Delta^{12}CH_2D_2$ produced from running a forward model using Inversion_base's posteriors are shown in Figure 2. For all the isotopic ratio plots, the spacing between horizontal grey lines represents our estimate of the likely maximum difference that could be observable between two measured trends. We estimate these to be 0.04 ‰, 2 ‰, 0.4 ‰, and 1.2 ‰ for $\delta^{13}C$, δD, $\Delta^{13}CH_3D$ and $\Delta^{12}CH_2D_2$, respectfully. These are derived by assuming a measurement uncertainty (0.02 ‰, 1 ‰, 0.2 ‰ and 0.6 ‰ for $\delta^{13}C$, δD, $\Delta^{13}CH_3D$ and $\Delta^{12}CH_2D_2$, respectfully) and including two error propagation steps for transferring an international scale reference to the air measurement. The assumed measurement

uncertainties for singly-substituted isotopologues are taken from the WMO/GAW network compatibility goals (World Meteorological Organization, 2018), which are at a level representative of the best precisions currently attainable by lower resolution IRMS. Those for clumped isotopologues are from the attainable measurement precision demonstrated by HR-IRMS for measurements of higher concentration natural or synthetic samples (Young et al., 2017). It should be noted that HR-IRMS instruments for clumped CH_4 analysis make far more precise measurements of $\delta^{13}C$ and δD compared to the more common lower resolution IRMS techniques. These further gains in precision of $\delta^{13}C$ and δD by HR-IRMS, however, would currently be unlikely to equate to improved CH_4 budget constraints, especially at the frequency at which measurements are currently feasible. Improving measurement coverage (in time and space), improving the atmospheric chemistry transport modelling of isotope ratios, and reducing uncertainties in the source signatures are all other avenues being explored to bring greater constraints on the global methane budget from $\delta^{13}C$ and δD measurements.

Our aim here is not to produce another inverse result of global sources and sinks of CH_4 but firstly to demonstrate that our results are comparable to studies made thus far and to verify our modelling and inversion approach. For the purpose of our study Inversion_base is essentially a calibration of the model OH concentration, emissions and source isotopic signatures for the following modelling studies that follow (Table 1). Although we estimate a lower concentration of OH across the time series compared to our prior, we do not detect a trend in this over time. Turner et al. (2017) used independent box modelling approaches and also showed that the OH concentration could remain constant while explaining the available observations (within very feasible uncertainty limits of observations and prior information). Regarding emissions, we observe an increase in the global emissions from 516 (486-547) Tg yr^{-1} to 568 (537-598) Tg yr^{-1} between 2000 and 2015. These estimates are generally slightly smaller than other studies (e.g. Rigby et al. (2017), Saunois et al. (2016)), however, they are well within the likely uncertainty of global CH_4 emissions, which provides confidence that our inversion model setup is suitable for a study on projecting the likely magnitudes of clumped isotope signatures and trends in the atmosphere.

Table 1. Descriptions of the model studies conducted.

Model study name	Description
Inversion_base	Initial inversion using measurements and prior information to create a set of posterior estimates of emissions, OH anomaly, and $\delta^{13}C$ and δD source signatures. The median observation vector from the inversion is used as the 'pseudo-observation' dataset for following experiments.
Forward_OH_inc	Forward model run using median posterior state vector of Inversion_base as model input except OH anomaly increasing between the median (in 1980) and the 84th percentile (in 2015) of Inversion_base's posterior.
Forward_OH_dec	Same as Forward_OH_inc, but with OH anomaly decreasing between the median (in 1980) and the 16th percentile (in 2015) of Inversion_base's posterior.
Forward_Q_inc	Same as Forward_OH_inc, but with equivalent changes in emissions instead of OH.
Forward_Q_dec	Same as Forward_OH_dec, but with equivalent changes in emissions instead of OH.
Forward_Qff_inc	Same as Forward_Q_inc, but considering the emissions increase is due to increased fossil fuel emissions only.
Forward_Qff_dec	Same as Forward_Q_dec, but considering the emissions decrease is due to decreased fossil fuel emissions only.
Inversion_fixQ	Same inversion setup as the Inversion_base but with emissions fixed to prior.
Inversion_fixOH	Same inversion setup as the Inversion_base but with OH fixed to prior.

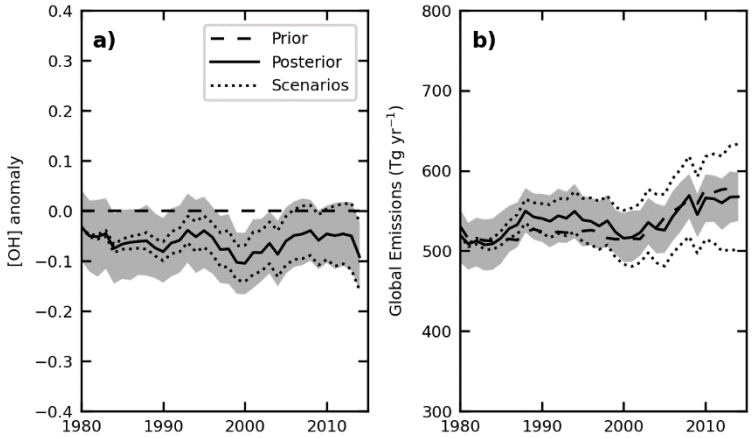

Figure 1. Prior (dashed) and posterior (solid) a) annual global OH anomaly and b) annual global total emissions from Inversion_base. Source signature time series are given in the supporting information. The uncertainty on the posterior, shown as a shaded area, represents the 16th to 84th percentiles (~1 sigma). The dotted lines represent the changes in OH and global emissions used in the further modelling scenarios described in Table 1.

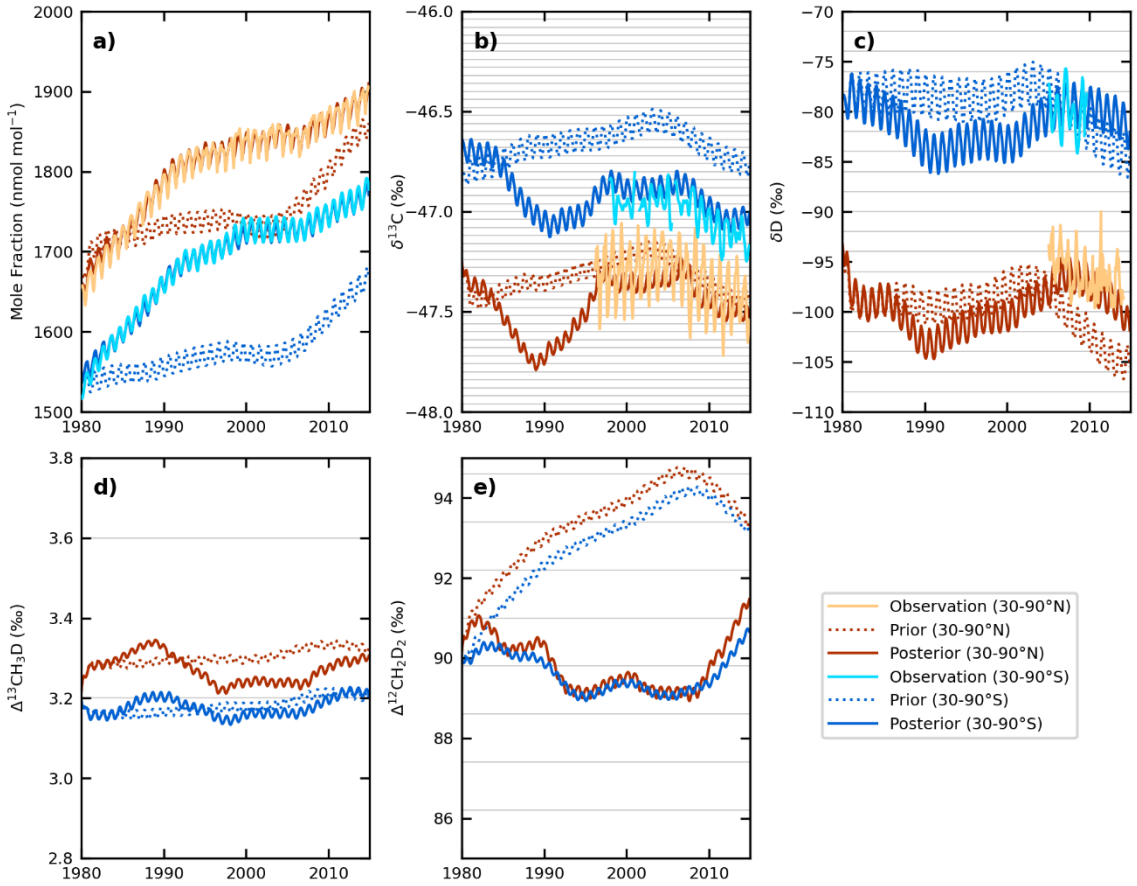

Figure 2. Modelled mixing ratios and isotopologue ratios using prior (darker dotted line) and median posterior (darker solid line) state vector from Inversion_base scenario. Measurements are shown in the lighter solid line. Grey horizontal lines represent estimates

of maximum observable differences across trends given current measurement capabilities: 0.04 ‰, 2 ‰, 0.4 ‰, and 1.2 ‰ for $\delta^{13}C$, δD, $\Delta^{13}CH_3D$ and $\Delta^{12}CH_2D_2$, respectfully.

Our second aim for Inversion_base was to create a pseudo-observation data set (and state data set) that filled in any measurement gaps in our time period of study (1980-2015), which particularly concerns δD. To this end, the median posterior from Inversion_base is used as the subsequent observation vector for two further inversion experiments (Inversion_fixQ and Inversion_fixOH). The use of a derived pseudo-observation data set ensured that the changes in the clumped CH_4 cannot simply be explained by changes in estimates of $\delta^{13}C$ and δD where real measurement gaps exist.

For clarity we focus the analysis of our results on the extratropical Northern and Southern Hemisphere boxes. Tropical boxes, displayed in the supporting material, show similar behaviours as the extratropics, not only in the inversion, but also in the prior runs. Model output shows a seasonal cycle in mixing ratio, $\delta^{13}C$ and δD largest in the northern tropics, which is in line with observations.

We can compare the general magnitude of our results of the clumped isotopes to that of Haghnegahdar et al. (2017). Haghnegahdar et al. [2017] use a one box model to calculate a steady state $\Delta^{13}CH_3D$ of 4.5 ‰, which is higher than our estimates of between 3.1 and 3.3 ‰ (depending on the hemisphere and the input flux parameters). This can be attributed to our use of a lighter global source signature for $\Delta^{13}CH_3D$ compared to Haghnegahdar et al. [2017]. We verified this by through a separate inverse model run using the source signature of Haghnegahdar et al. [2017], resulting in atmospheric values of 4.4-4.7 ‰ and around the same as estimates by Haghnegahdar et al. [2017] of 4.5 ‰ (see supporting information, Figures S11 and S12).

Haghnegahdar et al. [2017] estimated a steady state $\Delta^{12}CH_2D_2$ of 113.5 ‰, however, we calculate a much lighter atmosphere (between 89 and 92 ‰). Haghnegahdar et al. [2017] also estimate quite a heavy value for δD of more than −60 ‰, compared to our estimates from the inversion that are close to the measured values ~ −90 ‰. Both $\Delta^{12}CH_2D_2$ and δD are significantly influenced by fractionation during destruction in the atmosphere and therefore the discrepancy between studies is likely due to the balance of source and sink

magnitudes used, with our flux magnitudes being informed by the atmospheric measurements.

Looking at the difference between our prior and posterior trends, it appears that significant differences can be seen between $\delta^{13}C$, δD and $\Delta^{12}CH_2D_2$, however, no difference for $\Delta^{13}CH_3D$ would be measurable given the current precision of measurements. The seasonal cycles for both $\Delta^{13}CH_3D$ and $\Delta^{12}CH_2D_2$ are surprisingly small and are probably not detectable. The resulting $\Delta^{13}CH_3D$ shows a particularly small seasonal cycle relative to measurement precision (average of 0.03 ‰) compared to around 0.2 ‰ predicted by Whitehill et al. (2017). We have also used the closed system model using Rayleigh distillation formula under the same settings as Whitehill et al. (2017), however, we calculate a seasonal cycle amplitude of only 0.02 ‰ in line with our atmospheric model output (further details of this calculation are given in the supporting information).

Our model is a simplification of atmospheric transport and ignores significant spatial and temporal variability in sources and sinks, however, the seasonal cycles for $\delta^{13}C$ and δD are only slightly smaller than measured values. We therefore do not expect that the amplitude of the seasonal cycles in the atmosphere for $\Delta^{13}CH_3D$ and $\Delta^{12}CH_2D_2$ to deviate significantly from our model estimates. Like $\Delta^{13}CH_3D$, the closed system model using the Rayleigh distillation formula gave a seasonal cycle of $\Delta^{12}CH_2D_2$ of 0.19 ‰, which is similar to our model results between mid-1990s and mid-2000s when modelled $\Delta^{12}CH_2D_2$ was stable.

The seasonal cycle for $\Delta^{12}CH_2D_2$ is particularly small compared to the relatively large changes in the longer-term trends. This is an interesting result that could have implications for measurement interpretation. In many global studies of CH_4 concentrations and $\delta^{13}C$, seasonal cycles are often ignored by annually averaging the measurements at latitudinal bands in order to be easily interpret long term trends. This result suggests that fewer measurements of $\Delta^{12}CH_2D_2$ would be needed compared to $\delta^{13}C$ (and δD if the monthly observations were to resume) in order to derive accurate estimates of annual averages, which is important given the expected cost and difficulty in making these measurements.

4.2 Forward model sensitivity tests

We ran our model using the posterior estimates from Inversion_base as the default values for CH_4 emission rates, source isotope signatures and OH anomaly. Deviations from these Inversion_base posterior default values were used to demonstrate how changes in sources or sinks influenced the modelled CH_4 burden and isotopologue ratios (these tests are listed in Table 1 with a prefix "Forward_").

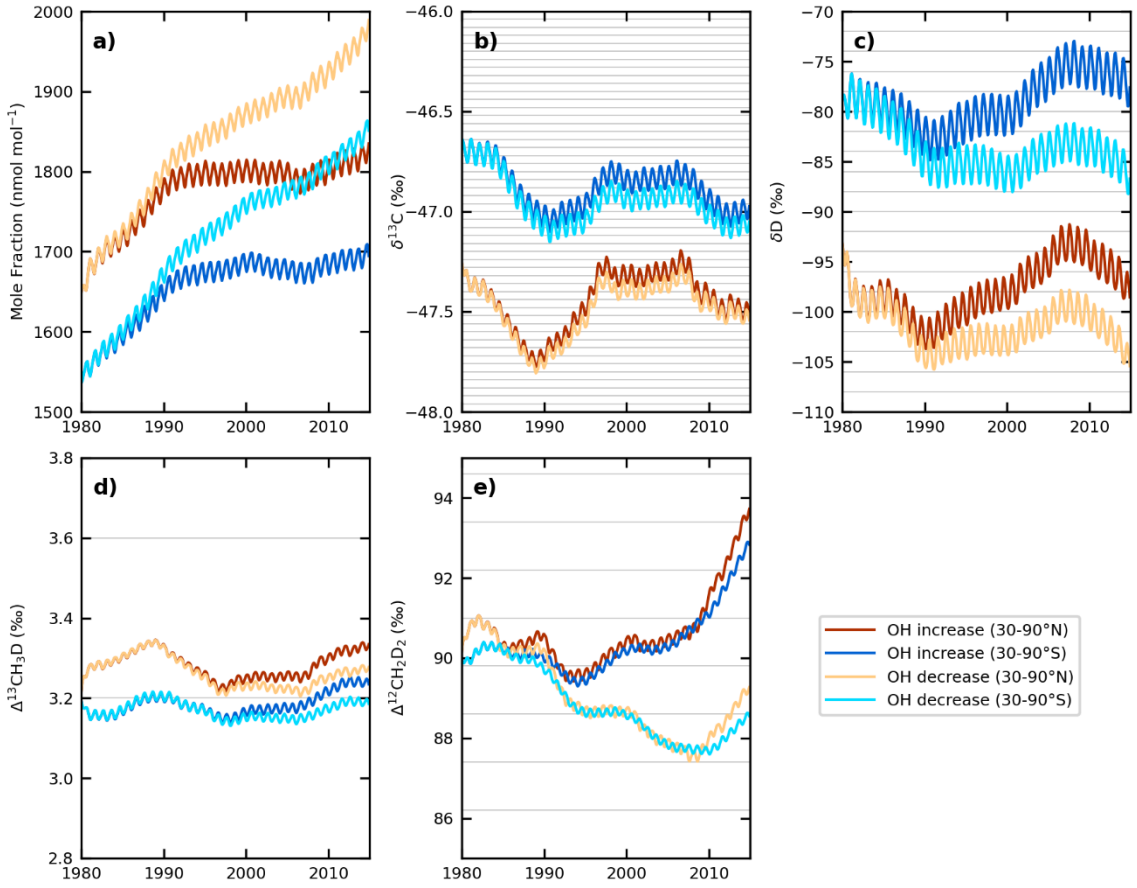

Figure 3. Modelled mixing ratios and isotopologue ratios from scenarios Forward_OH_inc (darker lines) and Forward_OH_dec (lighter lines). Grey horizontal lines as described in Figure 2.

Experiments Forward_OH_inc and Forward_OH_dec (Figure 3) demonstrate the effect of increasing or decreasing the main sink – reaction with OH. An increase in sink (issued by an increase in the OH abundance) led to a generally heavier atmospheric CH_4 burden since kinetically controlled reactions preferentially rupture bonds of lighter isotopes. The trends in the four different isotopologue ratios, however, showed significant deviations in behaviour. $\delta^{13}C$ showed changes that would be difficult to detect in the atmosphere despite the CH_4 burden changing by over 100 ppb between the two sink scenarios. δD showed larger differences

compared to $\delta^{13}C$ considering the attainable measurement uncertainty, suggesting that improving global long-term monitoring of δD could improve constraints in the atmosphere's oxidative capacity. It should be noted, however, that the sign of the trend's gradient was consistent in the scenarios across the full time series indicating that improved knowledge of source signatures would likely to be needed for full interpretation. $\Delta^{13}CH_3D$ showed minimal difference between scenarios, in line with findings from the Inversion_base inversion that $\Delta^{13}CH_3D$ would provide little further constraints on understanding atmospheric CH_4. Deviations in $\Delta^{12}CH_2D_2$ between scenarios were both significant and showed periods where the sign of the trend deviated. Between 1998 and 2003 $\Delta^{12}CH_2D_2$ moved lighter with a smaller sink but heavier with a larger sink. The contrast between simulated trends in $\Delta^{13}CH_3D$ and $\Delta^{12}CH_2D_2$ is notable. Only minor, insignificant deviations in the ambient $\Delta^{13}CH_3D$ trend (even with relatively large changes in sink regime) is commensurate with the fact that the reaction rate of $^{13}CH_3D$ with OH does not significantly deviate from what would be extrapolated from reaction rates of $^{13}CH_4$ and $^{12}CH_3D$ with OH (Whitehill et al., 2017).

In a second set of sensitivity tests we looked at the impact of changing emissions and changing emissions source on the evolving isotopic signatures. Experiments Forward_Q_inc and Forward_Q_dec (Figure 4) are analogous to Forward_OH_inc and Forward_OH_dec, however, in Forward_Q_inc and Forward_Q_dec the global emissions were perturbed instead of the OH sink as explained in Table 1. In Forward_Qff_inc and Forward_Qff_dec the change in emissions were assigned only to the fossil fuel sector.

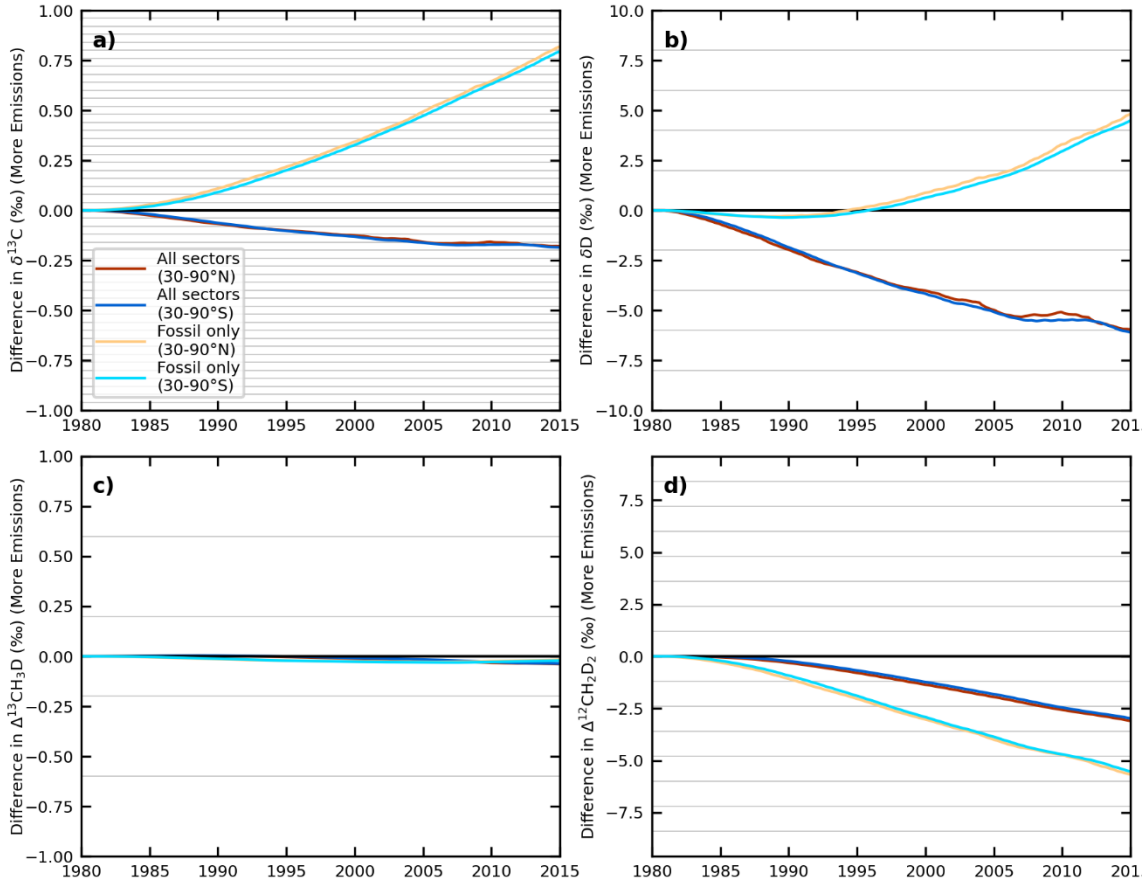

Figure 4. The difference between the median modelled time series from Inversion_base and the forward models under increasing emission scenarios (darker lines for Forward_Q_inc and lighter lines for Forward_Qff_inc). Four pairs of plots are for each of the four modelled isotopologue ratios: a) $\delta^{13}C$, b) δD, c) $\Delta^{13}CH_3D$ and d) $\Delta^{12}CH_2D_2$. Grey horizontal lines as described in Figure 2.

The results from sensitivity tests labelled under Forward_Q_inc/dec and Forward_Qff_inc/dec (as equivalently presented in Figure 3 for Forward_OH_inc/dec) are provided in the supporting information. In Figure 4 we illustrate the difference in the evolving isotope signature over 35 years between our best estimate (from Inversion_base) and each of two sensitivity tests: increasing emissions from global mixed sources (Forward_Q_inc) or increasing emissions from fossil sources only (Forward_Qff_inc) as described in Table 1. Decreasing emissions from global mixed sources (Forward_Q_dec) and decreasing emissions from fossil sources only (Forward_Qff_dec) showed the opposite trends to Forward_Q_inc and Forward_Qff_inc, respectively (Figure S10).

The already significant potential for the traditional bulk isotope ratios to understand changes in sources is clear. $\delta^{13}C$ and δD move towards distinctly heavier atmospheric compositions when fossil sources are increased but when a mixed source is increased (containing significant lighter microbial emissions) the atmosphere moves lighter. $\Delta^{13}CH_3D$, however, shows no trend that would be detectable in the atmosphere, likely due to difference between overall source signatures and the atmosphere being small. In contrast, atmospheric $\Delta^{12}CH_2D_2$, moves positive with decreasing global emissions independent of the source. This means that, unlike the bulk isotope ratios, interpretation of $\Delta^{12}CH_2D_2$ could be based largely on changes in the global source or sink with less concern for the uncertainty in emissions sector mix or the isotopic signature of specific sectors. It is noteworthy that $\Delta^{13}CH_3D$ still remains largely unperturbed in relation to a measurable signature in the atmosphere – all modelled scenarios lie within the analytical uncertainty of measurement.

4.3 Inversion experiments with altered OH and emissions pathways

We conducted a further inversion (based on the method used to generate results under section 4.1) to understand if the large changes in $\Delta^{12}CH_2D_2$ observed in the forward model runs under section 4.2 can be translated into potentially useful observables for global inverse modelling of the CH_4 cycle.

These inversions use the pseudo-observations generated by Inversion_base as the observation vector (Table 1). However, unlike the Inversion_base, test Inversion_fixQ only allows the OH anomaly to vary (with emissions fixed to the prior) and Inversion_fixOH only allows emissions to vary (with the OH anomaly fixed to the prior – an OH anomaly fixed to zero from 1980).

The results displayed in Figure 5 show that, as expected, the inversion gave lower emissions in lower sink environment, and higher emissions in higher sink environment. Both inversions were able to reproduce the pseudo-observation data sets (Figure 6 a,b,c). For the ambient clumped isotopic signatures, $\Delta^{13}CH_3D$ shows negligible difference between the two different sink scenarios (Figure 6d), which was expected since little change was observed in relevant individual sensitivity tests (Forward_OH_inc, Forward_OH_dec, Forward_Q_inc and Forward_Q_dec) performed in the simple forward model runs in the previous section.

$\Delta^{12}CH_2D_2$, which showed meaningful deviations in the previous forward model tests, showed smaller differences in the inversion results, but with detectable deviations developing once annual OH anomalies reached ~10 % (Figure 6e). The scenario with no interannual variation of OH (Inversion_fixOH) resulted in heavier $\Delta^{12}CH_2D_2$, than when emission amount was fixed (and leading to a reduction in the OH from 1980). As the OH anomaly rose back to zero towards the end of the time series the deviation between Inversion_fixQ and Inversion_fixOH decreased. This result shows that possible realistic changes in OH developed over years to decades would result in measurable changes in $\Delta^{12}CH_2D_2$ in the atmosphere.

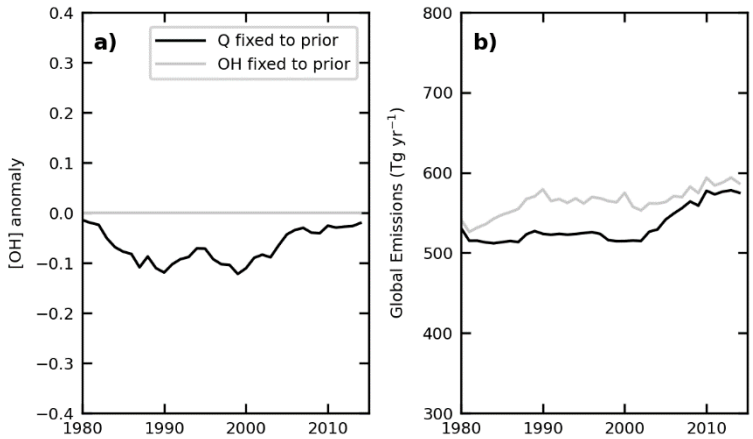

Figure 5. Median posteriors of a) annual global OH anomalies and b) total emissions from scenarios Inversion_fixQ (dark), Inversion_fixOH (light).

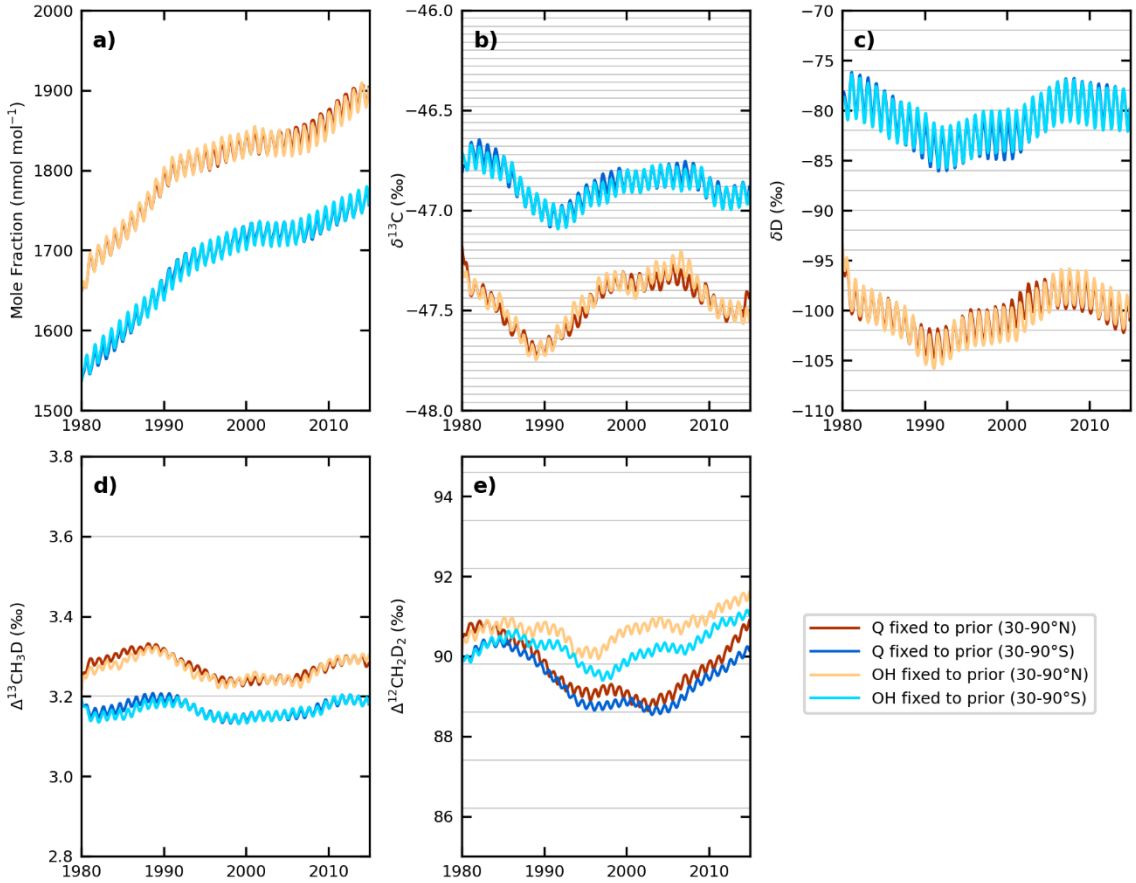

Figure 6. Modelled observations using median posterior state vectors from scenarios Inversion_fixQ (dark) and Inversion_fixOH (light). Grey horizontal lines as described in Figure 2.

5 Conclusion

In this study, we explored different source and sink scenarios, and using an inverse method we estimate the changes in CH_4's clumped isotope ratios in ambient air that could be expected given modest changes in the global source-sink balance. As in other global studies we show that current observables (mixing ratio, $\delta^{13}C$, δD) alone cannot adequately constrain the CH_4 budget or determine whether the current trends (recent decades) are driven by changes in emissions or the oxidative capacity of the atmosphere. Modelling of $\Delta^{12}CH_2D_2$ demonstrated a small but important trait, where a larger global source and sink scenario resulted in a move towards a heavier ambient $\Delta^{12}CH_2D_2$ than a lower emission-lower sink scenario (with both systems adequately explained using current observation data sets). We also estimate that the seasonal variability for $\Delta^{12}CH_2D_2$ is smaller than the modelled deviations in longer term trends (unlike as observed with the bulk isotope ratios). Thus, fewer measurements might be necessary

to define and be confident of a long-term trend, which will be important given the ultimate cost and effort that would be needed to make these measurements.

It is also worth noting that this study has only considered small and gradual changes in the source-sink balance over decades. Possible abrupt perturbations in the Earth system that could cause a step change to the CH_4 cycle, need to be considered in future monitoring strategies. To this end, measurements of $\Delta^{12}CH_2D_2$ could provide a highly valuable extra observable. Atmospheric air archives have been used to construct the histories of gases and isotope ratios going back several decades once new techniques have been developed. Measurements of these clumped isotopes, however, would require hundreds of litres of samples and therefore future measurement techniques will need to be fully demonstrated and tested before this is attempted.

Our results are dependent on very few measurements and calculations of the KIEs for $\Delta^{13}CH_3D$ and $\Delta^{12}CH_2D_2$. Thus, alongside a concerted effort to make measurements of ambient air, commensurate improvements in our understanding of the source and sink signatures are needed before clumped isotopes become a part of the armoury for interpreting global CH_4.

Acknowledgements

This work is supported by National Measurement System funding to the National Physical Laboratory (NPL) in the UK and through strategic research funding streams within NPL. Edward Chung was supported by a PhD studentship funded by the University of Edinburgh and NPL. The Natural Environment Research Council (NERC) project POLYGRAM: POLYisotopologues of Greenhouse gases: Analysis and Modelling (NE/V007149/1) also supported this study We thank the networks (AGAGE and NOAA ESRL) and INSTAAR laboratory for ongoing meticulous monitoring efforts that are responsible for our current understanding of CH_4 in the global atmosphere, and for making their data publicly available for studies such as this one. We thank Dr Shinji Morimoto from Tohoku University and Dr Ryo Fujita from Meteorological Research Institute for providing us with their $\delta^{13}C$ and δD measurement data for this study. We thank Dr Matt Rigby at the University of Bristol for discussions regarding the 12-box model. Datasets for this research are available in these in-text data citation references: Meinshausen et al., (2017), White et al., (2016; 2017), Fujita et al. (2018) and Morimoto et al. (2017). We would also like to thank Dr Peter Douglas and an

anonymous reviewer for their time spent reviewing our submission and ultimately improving the paper.

References

Bloom, A. A., K. W. Bowman, M. Lee, A. J. Turner, R. Schroeder, J. R. Worden, R. Weidner, K. C. McDonald, and D. J. Jacob (2017), A global wetland methane emissions and uncertainty dataset for atmospheric chemical transport models (WetCHARTs version 1.0), Geosci. Model Dev., 10(6), 2141-2156, doi: 10.5194/gmd-10-2141-2017.

Chipperfield, M. P., and Q. Liang (2013), SPARC Lifetimes Report (2013) – SPARC Report No. 6*Rep.*

Cunnold, D. M., P. J. Fraser, R. F. Weiss, R. G. Prinn, P. G. Simmonds, B. R. Miller, F. N. Alyea, and A. J. Crawford (1994), Global trends and annual releases of CCl_3F and CCl_2F_2 estimated from ALE/GAGE and other measurements from July 1978 to June 1991, J. Geophys. Res.-Atmos., 99(D1), 1107–1126, doi: 10.1029/93jd02715.

Dlugokencky, E. J., A. M. Crotwell, J. W. Mund, M. J. Crotwell, and K. W. Thoning (2020), Atmospheric Methane Dry Air Mole Fractions from the NOAA GML Carbon Cycle Cooperative Global Air Sampling Network, 1983-2019, Version: 2020-07, edited.

Douglas, P. M. J., et al. (2020), Clumped Isotopes Link Older Carbon Substrates With Slower Rates of Methanogenesis in Northern Lakes, Geophys. Res. Lett., 47(6), e2019GL086756, doi: https://doi.org/10.1029/2019GL086756.

Douglas, P. M. J., et al. (2017), Methane clumped isotopes: Progress and potential for a new isotopic tracer, Organic Geochemistry, 113(Supplement C), 262-282, doi: https://doi.org/10.1016/j.orggeochem.2017.07.016.

Eiler, J. M. (2007), "Clumped-isotope" geochemistry—The study of naturally-occurring, multiply-substituted isotopologues, Earth and Planetary Science Letters, 262(3–4), 309-327, doi: http://dx.doi.org/10.1016/j.epsl.2007.08.020.

Etminan, M., G. Myhre, E. J. Highwood, and K. P. Shine (2016), Radiative forcing of carbon dioxide, methane, and nitrous oxide: A significant revision of the methane radiative forcing, Geophys. Res. Lett., 43(24), 12,614-612,623, doi: 10.1002/2016GL071930.

Eyer, S., et al. (2016), Real-time analysis of δ13C- and δD-CH4 in ambient air with laser spectroscopy: method development and first intercomparison results, Atmos. Meas. Tech., 9(1), 263-280, doi: 10.5194/amt-9-263-2016.

Fujita, R., S. Morimoto, T. Umezawa, K. Ishijima, P. K. Patra, D. E. J. Worthy, D. Goto, S. Aoki, and T. Nakazawa (2018), Temporal Variations of the Mole Fraction, Carbon, and Hydrogen Isotope Ratios of Atmospheric Methane in the Hudson Bay Lowlands, Canada,

Journal of Geophysical Research: Atmospheres, 123(9), 4695-4711, doi: doi:10.1002/2017JD027972.

Ganesan, A. L., et al. (2019), Advancing Scientific Understanding of the Global Methane Budget in Support of the Paris Agreement, Global Biogeochemical Cycles, 33(12), 1475-1512, doi: 10.1029/2018gb006065.

Gonzalez, Y., D. D. Nelson, J. H. Shorter, J. B. McManus, C. Dyroff, M. Formolo, D. T. Wang, C. M. Western, and S. Ono (2019), Precise measurements of 12CH2D2 by tunable infrared laser direct absorption spectroscopy, Analytical chemistry, 91(23), 14967-14974.

Goodman, J., and J. Weare (2010), Ensemble samplers with affine invariance, Commun. Appl. Math. Comput. Sci., 5(1), 65-80, doi: 10.2140/camcos.2010.5.65.

Haghnegahdar, M. A., E. A. Schauble, and E. D. Young (2017), A model for 12CH2D2 and 13CH3D as complementary tracers for the budget of atmospheric CH4, Global Biogeochemical Cycles, 31(9), 1387-1407, doi: 10.1002/2017GB005655.

Howarth, R. W. (2019), Ideas and perspectives: is shale gas a major driver of recent increase in global atmospheric methane?, Biogeosciences, 16(15), 3033-3046, doi: 10.5194/bg-16-3033-2019.

Janssens-Maenhout, G., et al. (2017), EDGAR v4.3.2 Global Atlas of the three major Greenhouse Gas Emissions for the period 1970-2012, Earth Syst. Sci. Data Discuss., 2017, 1-55, doi: 10.5194/essd-2017-79.

JPL (2013), ISLSCP II Land and Water Masks with Ancillary Data, edited, ORNL Distributed Active Archive Center.

Meinshausen, M., et al. (2017), Historical greenhouse gas concentrations for climate modelling (CMIP6), Geosci. Model Dev., 10(5), 2057-2116, doi: 10.5194/gmd-10-2057-2017.

Morimoto, S., R. Fujita, S. Aoki, D. Goto, and T. Nakazawa (2017), Long-term variations of the mole fraction and carbon isotope ratio of atmospheric methane observed at Ny-Ålesund, Svalbard from 1996 to 2013, Tellus B: Chemical and Physical Meteorology, 69(1), 1380497, doi: 10.1080/16000889.2017.1380497.

Nisbet, E. G., et al. (2019), Very Strong Atmospheric Methane Growth in the 4 Years 2014–2017: Implications for the Paris Agreement, Global Biogeochemical Cycles, 33(3), 318-342, doi: 10.1029/2018gb006009.

Nisbet, E. G., et al. (2016), Rising atmospheric methane: 2007–2014 growth and isotopic shift, Global Biogeochemical Cycles, 30(9), 1356-1370, doi: 10.1002/2016GB005406.

Ono, S., D. T. Wang, D. S. Gruen, B. Sherwood Lollar, M. S. Zahniser, B. J. McManus, and D. D. Nelson (2014), Measurement of a Doubly Substituted Methane Isotopologue, 13CH3D, by Tunable Infrared Laser Direct Absorption Spectroscopy, Analytical Chemistry, 86(13), 6487-6494, doi: 10.1021/ac5010579.

Patra, P. K., et al. (2014), Observational evidence for interhemispheric hydroxyl-radical parity, Nature, 513(7517), 219-223, doi: 10.1038/nature13721.

Prinn, R. G., et al. (2018), History of chemically and radiatively important atmospheric gases from the Advanced Global Atmospheric Gases Experiment (AGAGE), Earth Syst. Sci. Data, 10(2), 985-1018, doi: 10.5194/essd-10-985-2018.

Rennick, C., T. Arnold, E. Safi, A. Drinkwater, C. Dylag, E. M. Webber, R. Hill-Pearce, D. R. Worton, F. Bausi, and D. Lowry (2021), Boreas: A Sample Preparation-Coupled Laser Spectrometer System for Simultaneous High-Precision In Situ Analysis of δ13C and δ2H from Ambient Air Methane, Analytical Chemistry, 93(29), 10141-10151, doi: 10.1021/acs.analchem.1c01103.

Rice, A. L., C. L. Butenhoff, D. G. Teama, F. H. Röger, M. A. K. Khalil, and R. A. Rasmussen (2016), Atmospheric methane isotopic record favors fossil sources flat in 1980s and 1990s with recent increase, Proceedings of the National Academy of Sciences, 113(39), 10791-10796, doi: 10.1073/pnas.1522923113.

Rigby, M., et al. (2013), Re-evaluation of the lifetimes of the major CFCs and CH_3CCl_3 using atmospheric trends, Atmos. Chem. Phys., 13(5), 2691-2702, doi: 10.5194/acp-13-2691-2013.

Rigby, M., et al. (2017), Role of atmospheric oxidation in recent methane growth, Proceedings of the National Academy of Sciences, 114(21), 5373-5377, doi: 10.1073/pnas.1616426114.

Röckmann, T., M. Brass, R. Borchers, and A. Engel (2011), The isotopic composition of methane in the stratosphere: high-altitude balloon sample measurements, Atmos. Chem. Phys., 11(24), 13287-13304, doi: 10.5194/acp-11-13287-2011.

Röckmann, T., et al. (2016), In situ observations of the isotopic composition of methane at the Cabauw tall tower site, Atmos. Chem. Phys., 16(16), 10469-10487, doi: 10.5194/acp-16-10469-2016.

Saunois, M., P. Bousquet, B. Poulter, A. Peregon, P. Ciais, J. G. Canadell, E. J. Dlugokencky, G. Etiope, D. Bastviken, and S. Houweling (2016), The global methane budget 2000–2012, Earth System Science Data, 8(2), 697-751.

Schaefer, H., et al. (2016), A 21st-century shift from fossil-fuel to biogenic methane emissions indicated by $^{13}CH_4$, Science, 352(6281), 80-84, doi: 10.1126/science.aad2705.

Schwietzke, S., et al. (2016), Upward revision of global fossil fuel methane emissions based on isotope database, Nature, 538(7623), 88-91.

Sherwood, O. A., S. Schwietzke, V. A. Arling, and G. Etiope (2017), Global Inventory of Gas Geochemistry Data from Fossil Fuel, Microbial and Burning Sources, version 2017, Earth Syst. Sci. Data, 9(2), 639-656, doi: 10.5194/essd-9-639-2017.

Shindell, D., et al. (2012), Simultaneously Mitigating Near-Term Climate Change and Improving Human Health and Food Security, Science, 335(6065), 183-189, doi: 10.1126/science.1210026.

Snover, A. K., P. D. Quay, and W. M. Hao (2000), The D/H content of methane emitted from biomass burning, Global Biogeochemical Cycles, 14(1), 11-24, doi: 10.1029/1999gb900075.

Spivakovsky, C. M., et al. (2000), Three-dimensional climatological distribution of tropospheric OH: Update and evaluation, Journal of Geophysical Research: Atmospheres, 105(D7), 8931-8980, doi: 10.1029/1999jd901006.

Stolper, D. A., A. L. Sessions, A. A. Ferreira, E. V. Santos Neto, A. Schimmelmann, S. S. Shusta, D. L. Valentine, and J. M. Eiler (2014), Combined 13C–D and D–D clumping in methane: Methods and preliminary results, Geochimica et Cosmochimica Acta, 126, 169-191, doi: http://dx.doi.org/10.1016/j.gca.2013.10.045.

Turner, A. J., C. Frankenberg, and E. A. Kort (2019), Interpreting contemporary trends in atmospheric methane, Proceedings of the National Academy of Sciences, 116(8), 2805-2813, doi: 10.1073/pnas.1814297116.

Turner, A. J., C. Frankenberg, P. O. Wennberg, and D. J. Jacob (2017), Ambiguity in the causes for decadal trends in atmospheric methane and hydroxyl, Proceedings of the National Academy of Sciences, 114(21), 5367-5372, doi: 10.1073/pnas.1616020114.

van der Werf, G. R., et al. (2017), Global fire emissions estimates during 1997–2016, Earth Syst. Sci. Data, 9(2), 697-720, doi: 10.5194/essd-9-697-2017.

Wang, D. T., et al. (2015), Nonequilibrium clumped isotope signals in microbial methane, Science, 348(6233), 428-431, doi: 10.1126/science.aaa4326.

Wang, Z., E. A. Schauble, and J. M. Eiler (2004), Equilibrium thermodynamics of multiply substituted isotopologues of molecular gases, Geochimica et Cosmochimica Acta, 68(23), 4779-4797, doi: http://dx.doi.org/10.1016/j.gca.2004.05.039.

Welp, L. R., R. F. Keeling, H. A. J. Meijer, A. F. Bollenbacher, S. C. Piper, K. Yoshimura, R. J. Francey, C. E. Allison, and M. Wahlen (2011), Interannual variability in the oxygen isotopes of atmospheric CO2 driven by El Niño, Nature, 477(7366), 579-582, doi: 10.1038/nature10421.

White, J. W. C., B. H. Vaughn, and S. E. Michel (2016), University of Colorado, Institute of Arctic and Alpine Research (INSTAAR), Stable Isotopic Composition of Atmospheric Methane (2H) from the NOAA ESRL Carbon Cycle Cooperative Global Air Sampling Network, 2005-2009, Version: 2016-04-26, edited, ftp://aftp.cmdl.noaa.gov/data/trace_gases/ch4h2/flask/.

White, J. W. C., B. H. Vaughn, and S. E. Michel (2017), University of Colorado, Institute of Arctic and Alpine Research (INSTAAR), Stable Isotopic Composition of Atmospheric Methane (13C) from the NOAA ESRL Carbon Cycle Cooperative Global Air Sampling Network, 1998–2015, Version: 2017-01-20, edited, ftp://aftp.cmdl.noaa.gov/data/trace_gases/ch4c13/flask/.

Whitehill, A. R., L. M. T. Joelsson, J. A. Schmidt, D. T. Wang, M. S. Johnson, and S. Ono (2017), Clumped isotope effects during OH and Cl oxidation of methane, Geochimica et Cosmochimica Acta, 196, 307-325, doi: http://dx.doi.org/10.1016/j.gca.2016.09.012.

World Meteorological Organization (2018), 19th WMO/IAEA Meeting on Carbon Dioxide, Other Greenhouse Gases and Related Measurement Techniques (GGMT-2017)*Rep*.

Young, E. D., D. Rumble III, P. Freedman, and M. Mills (2016), A large-radius high-mass-resolution multiple-collector isotope ratio mass spectrometer for analysis of rare isotopologues of O2, N2, CH4 and other gases, International Journal of Mass Spectrometry, 401, 1-10, doi: http://dx.doi.org/10.1016/j.ijms.2016.01.006.

Young, E. D., et al. (2017), The relative abundances of resolved 12CH2D2 and 13CH3D and mechanisms controlling isotopic bond ordering in abiotic and biotic methane gases, Geochimica et Cosmochimica Acta, 203, 235-264, doi: http://doi.org/10.1016/j.gca.2016.12.041.